

## **Critical issues in the application of Stereo-PIV in large hydrodynamic facilities: study of a catamaran in steady drift**

**Falchi M, Grizzi S, Aloisio G, Felli M and Di Felice F**

INSEAN-CNR, Marine Technology Research Institute, Rome, Italy  
massimo.falchi@cnr.it

### **ABSTRACT**

Nowadays Stereo-PIV (SPIV) technique has reached a level of accuracy and precision suitable to a wide use in industrial facilities. Nonetheless, performing Stereo-PIV measurements in large hydrodynamic facilities for naval applications - *e.g.* large cavitation tunnels, towing tanks, maneuverability basins - still poses challenging operative, technical and theoretical problems; in these regards, solutions are required to assure good quality results when dealing with deep underwater conditions, reflections from the hull model, bubbly and two-phase flows, air-water interface and air bubbles entrapment by breaking waves, to name a few. In the present work, an underwater modular probe is introduced, designed to host all the electronic and optic hardware required to perform 3C-2D velocity measurements around surface and submersible models. In particular, an application to a test case is presented; a catamaran model advancing in steady drift at different angles and velocities is investigated to study the dynamics of the keel vortices generated along the demi-hulls and their interaction with the free surface.

### **INTRODUCTION**

In naval hydrodynamics, ship resistance and propulsion history can be divided in two parts, the first one prior to the mid-nineteenth century in which ship building was based mainly on experiences done on existing units bringing minor improvements and a second one in which standard experimental tests on scale models represented, and still do, a fundamental step in ship design. By considering that friction and wave-making resistance observe different scaling laws with velocity [1], William K. Froude understood the value of testing at model scale whose results, extrapolated at full scale, could lead to important savings in terms of time and costs. As a natural outcome, in 1872 at Torquay, England, the world's first model tank, with 85x11x3meter in length, breadth and depth, entered in service under his direction. In addition, he was involved in the design of the towing carriage and a propeller dynamometer to simultaneously measure thrust, torque and rotational speed of model propeller. In few decades, many countries realized their own facilities and model scale tests became a standard.

On the Froude path, to fully characterize the resistance of surface and submersible vehicles, and to dimension their propulsors, force measurements by means of dynamometers and force balances are required; the whole set of tests is composed by the model towing test (to characterize the resistance of the fully appended hull without propeller), open water test (to assess the propeller performance in terms of thrust, torque and efficiency) and self-propulsion test (to validate the capability of the propeller to exert the sufficient thrust to drive the whole hull-appendages-propeller with the propeller working at the selected rotational speed for the corresponding cruise velocity). Practically, dimensioning of marine vehicle propulsors is traditionally based upon global measurements, following the standards of the International Towing Tank Conference.

Nowadays, considering that 95% of world trade is transported by ships, with an increase of 2% per year of transported goods, data of 1998 [1], increasingly demanding rules and classification standards have to be complied to reduce underwater noise as well as water and atmospheric pollution; on the other hand, to meet market demands, innovative and higher performance vehicles are envisaged, looking for faster, larger, sustainable and quieter marine ships. To fulfill all these targets, traditional tools used in naval engineering are less and less adequate; in fact, even if global measurements are still important for the performance assessment of marine vehicles, new approaches, either experimental and numerical, able to give a deep insight into the hydrodynamic and hydroacoustic involved phenomena are now mandatory. Due to the impetuous development undergone by numerical techniques and innovative measuring techniques, the two-fold approach based on Computational Fluid Dynamics (CFD) and Experimental Fluid Dynamics (EFD) allows investigations in fine details; fine experimental data, in fact, can describe quantitatively the flow structure and can be used for the validation of the numerical results as well. Among the experimental techniques, velocity evaluating tools are of particular interest in hydrodynamics due to their characteristic in unveiling the complex fluid flow structure.

About thirty years ago Particle Image Velocimetry (PIV) appeared for the first time in EFD, [2], as a promising technique capable to unveil coherent structures in a fluid flow; in fact, despite of its initial low spatial and velocity dynamic ranges, being inherently two-dimensional, simultaneous measurements in a properly illuminated and seeded planar region of interest were available.

Hot Wire Anemometry (HWA) and Laser Doppler Velocimetry (LDV), the state of the art techniques at that time, had, and still have, unequalled advantages; high sampling frequency, spatial resolution, and impressive signal-to-noise ratio for HWA, high velocity dynamic range and no calibration need for LDV, are the major benefits which make them undisputable for investigations in turbulence fluid flow and characterization of single-point statistics. Nevertheless, being point-wise techniques, the eduction of instantaneous vortex structures, ensemble flow features as well as spatial derivatives and cross-correlations is difficult or simply impossible.

The promise of evaluating instantaneously two- or three-components of velocity over many points in a plane made PIV and SPIV highly attractive to many researchers but many steps were still required before PIV could be considered a tool suitable to a wide and reliable use in fluid dynamics. Increasing the accuracy and precision of the technique, as well as versatility in terms of spatial and velocity resolution, have been the main goals to be achieved for many researchers worldwide. In the mid- 80's, a lot of confusion reigned regarding the optimal PIV system to be used; light source, image recording processing algorithm, data management, even seeding particles were all topics subjected to efforts in order to establish the best measuring solution [3]. The scenario dramatically changed with the advent of the digital age; digital cameras appeared, and double shutter ones in particular [4], and this boosted the development of new processing algorithms. Cross-correlation based algorithms proved to be more efficient and robust in comparison to auto-correlation ones [5]; successively, and rapidly, many further developments and refinements took place. Super-resolution PIV [6], [7], was introduced with the goal of obtaining one vector per particle emulating particle tracking but on a high seeding density; the procedure was based on a first interrogation over spots containing a sufficient number of particles to get a tentative reliable value to further pair particles and get one vector per pairs. Another proposed approach, hierarchical correlation method, based on decreasingly smaller spots using at each step as a first guess the vector evaluated at the previous one [8]. To copy with in-plane loss of pairs and consequently increase the cross-correlation peak evaluation, window offset and iterative window deformation algorithms have been introduced [9]; in a predictor-corrector scheme, the velocity field is first evaluated, interpolated on pixel basis on which both the first and second frames are deformed and then residual displacements are evaluated to refine the first value, applying these steps in an iterative way until the residual displacement is minor than a selected threshold. In these methods, interpolation and filtering schemes are of importance to assure convergence and increase the frequency response, [10], [11].

Using a single point of view, *i.e.* one camera, placed perpendicular to the light sheet, only two-components of velocity projection on that plane are evaluated; to eliminate projection error and determine an additional velocity component, a second point of view was introduced. From the two two-dimensional vector fields, a single three-components velocity field is reconstructed using a calibration to map the object space into the camera ones.

The so-called SPIV developed rapidly on the promise of evaluating three-components of velocity on a plane; taking advantage of all the efforts devoted in improving the accuracy of cross-correlation algorithms, in SPIV the attention was focused on optical set-ups, calibration algorithms and calibration correction schemes.

Regarding the optical set-up, two stereoscopic configurations were proposed; the translation method and the angular-displacement method. Anyhow the latter proved to reconstruct the out-of-plane component of velocity with a higher accuracy,[12], [13], and so it became widely accepted.

Being an essential prerequisite, most of the work has been devoted to calibration functions and different approaches have been proposed; camera pinhole model [14], rational functions derived from perspective equations [15], second-order or third-order polynomial functions in  $x$  and  $y$  [16], among the others. Definitely, Soloff's based method [16] is the one generally used; placing a calibration target in the  $z$ -coordinate of the laser light sheet ( $z=0$ ) and in additional  $z$  positions (at least an additional one), mapping functions are evaluated for the two cameras that warp from the  $x$ - $y$  object plane to the camera planes. The difference in the mapping functions between the  $z$  locations provide the  $z$  derivatives necessary to reconstruct the three velocity components. The main advantage of this empirical approach is that no information about the optical set-up are required and corrections for lens aberration, imperfections, multi-media distortions are accounted and compensated for in a single step. To correct the so-called "misregistration error", due to any misalignment between the position of the laser light sheet and the calibration target, a procedure based on the use of disparity maps, to refit the  $z=0$  plane to the position of the laser light sheet, was proposed, [17]; using this approach, accurate calibration is obtained even if the calibration target is far away from the position of the laser light sheet.

Nowdays SPIV, in addition to be considered a research tool suitable to complex turbulence investigations [18], is believed an accurate and reliable industrial instrument [19], [20]; anyhow, its use in large hydrodynamics facilities still poses a number of issues. Dealing with deep underwater conditions, reflections from models, bubbly and two-phase flows, air-water interface and air bubbles entrapment by breaking waves, reduced or absence of optical access are all problems that in a large naval facility has to be solved properly.

In this work, a review of issues and requirements for SPIV measurements in large hydrodynamic facilities is presented and an application to a test case, a catamaran in steady drift, is introduced; methods and materials, as well as results are reported. Finally, Conclusions are summarized.

## LARGE HYDRODYNAMIC FACILITIES: ISSUES AND REQUIREMENTS

In modern naval hydrodynamics, any sector needs experimental tests, so, to meet the various measuring purposes, dedicated facilities have been designed. In practice, all the facilities can be grouped in three sets: cavitation tunnels and channels, towing tanks and hydrodynamic basins. Different features can characterize one facility in respect to another of the same group (dimensions, presence of a wave generator, movable bottom, de- and pressurizing capacity, removable roof, free surface, etc) but each of them presents some general and common distinguishing one.

INSEAN-CNR hosts two towing tanks, a large cavitation tunnel and maneuverability basin which is actually a small lake with INSEAN exclusive use. Neglecting the latter, these experimental apparatus present huge dimensions suitable to test models ranging from 3 to 8 m in length.

Tank n. 1 is today one of the largest worldwide, Figure 1. It is 470 m long, 13.5 m wide and has a depth of 6.5 m. It is equipped with a towing carriage that can achieve a maximum speed of 15 m/s. Tank n. 2 is of smaller size, 220m long, 9 m wide and 3.8 m depth, and maximum carriage speed of 10 m/s. It is equipped with a single-flap wave generator, that provides regular as well as irregular waves for the investigation of sea-keeping characteristics and ride comfort. The towing tanks have many applications, mainly concerning resistance and propulsion tests for performance evaluation, 3-D wake surveys, vertical and horizontal planar motion experiments, resistance and hydrodynamic forces. The size of towing tank no. 1 offers excellent capabilities for the investigation of large, self-propelled models of high-speed vessels (mono- or multi-hull, semi-planing and planing craft, etc.). Equipment and methodologies for testing submarines and sail boats are available. Various unconventional marine vehicles can also be tested.

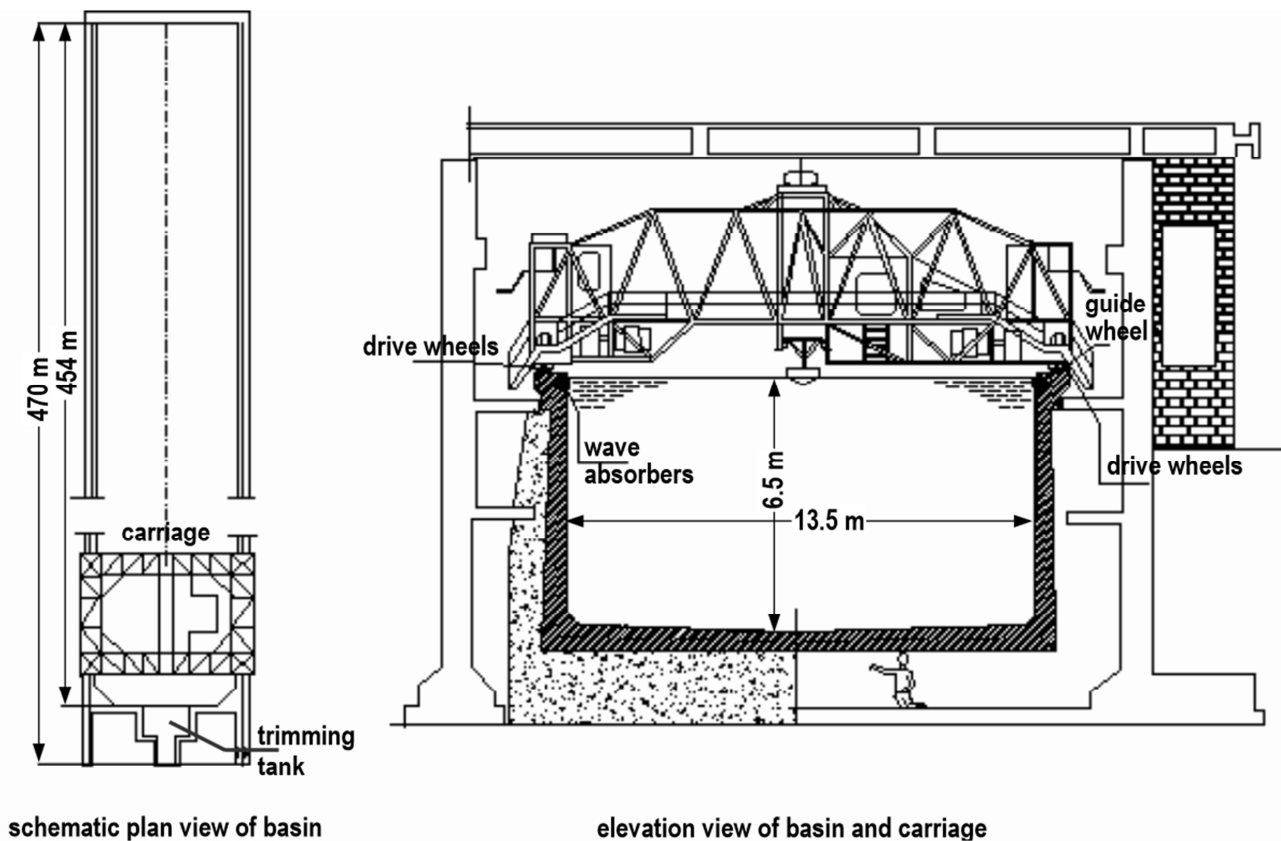


**Figure 1** Towing tank n. 1, schematic view.

The large cavitation channel (LCT) is a free-surface facility that can be de-pressurized, Figure 2. The test section is 10 m long, 3.6 m wide with a depth of 2.2 m. The maximum water speed is 5 m/s. The pressure in the test section can be reduced down to a minimum of 30 mbar. Due to a moveable cover, this facility can work as a closed jet type too. The total installed power is about 1 MW. Large perspex windows are available on three sides to allow optical access for visual inspection of the testing model, visualization and measurements from the adjacent rooms. This facility is used for cavitation observation tests, cavitation inception measurements, and performance tests with propellers in wake field behind the model; other suitable tests are hull pressure fluctuation measurements, propeller noise and radiated noise measurements, detailed flow measurements and so on.

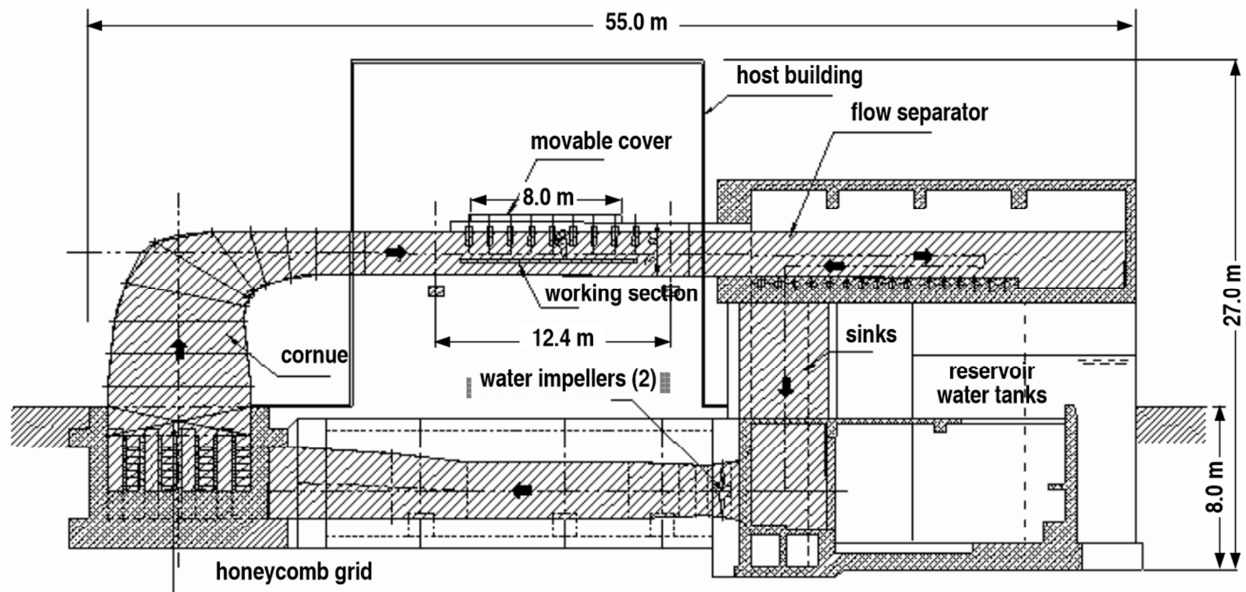


**Figure 2** Large cavitation tunnel, schematic view.

With reference to the aforementioned facilities, difficulties in performing SPIV measurements are immediately evident:

- the large dimensions involved together with the working fluid under consideration generate practical as well as technological problems that need a proper solutions.
- the presence of the free surface adds severe problems in terms of reflections at air-water interface, air entrapment and air bubbles due to wave breaking; in these conditions, image quality is highly decreased and, in the worst cases, damages to the sensors can arise.
- the reduced, or absence of, optical access due to the facility and model characteristics put other constraints to a SPIV measuring set-up.
- due to the extraordinary variety of applications, the investigation of some typical naval configurations such as submersible vehicles (i.e. submarine, underwater unmanned vehicle [UUV], remotely operated vehicle [ROV]) or multi-hull ships require a high level of adaptation of a SPIV system; high flexibility in optical camera configurations are also required.

The first question that needs to be addressed regards the kind of optical arrangement suitable to deal with the issues presented before. Setting up the SPIV system outside the test section, solution not suitable to the towing tank for absence of direct optical access, is to be considered a second choice; despite of the large Perspex windows, the positioning of the cameras is limited by the structure itself of the test section. In addition, the windows present an important thickness for resistance requirements when the apparatus is working at low pressure; this generates large aberrations at the air-glass-water interface, even when using prisms filled with water. Besides, in these measuring conditions the system is fixed; so when different region of interest have to be investigated, the model has to be displaced that is not completely free.

On the other hand, using a mixed system, one camera housed in water proof case immersed in the flow and one in dry as in [19], Figure 3, poses the same problems and adds misalignment problem due to relative motion between the “wet” camera and the laser light sheet.

An alternative solution is to house all the system aboard the model; anyhow, difficulties in mounting, calibrating and measuring are still present and, being on board, no relative displacement between the system and the model is possible, limiting the investigation to a single region. In case of investigation on large areas, different positions of the system have to be foreseen, increasing apparatus occupation and related costs.

A definitive solution is to place to whole SPIV system immersed in the flow in a stand-alone probe that can be calibrated at the beginning of the test campaign and translated in the test section through a devoted traversing system. Using this approach, once the optical configuration has been selected, the calibration can be performed and holds for all the test campaign, no matter the relative movements between the probe and the model. In this way many successive regions of interest can be investigated separately and assembled at the end of the processing procedure obtaining a spatial resolution as fine as desired on a large area.

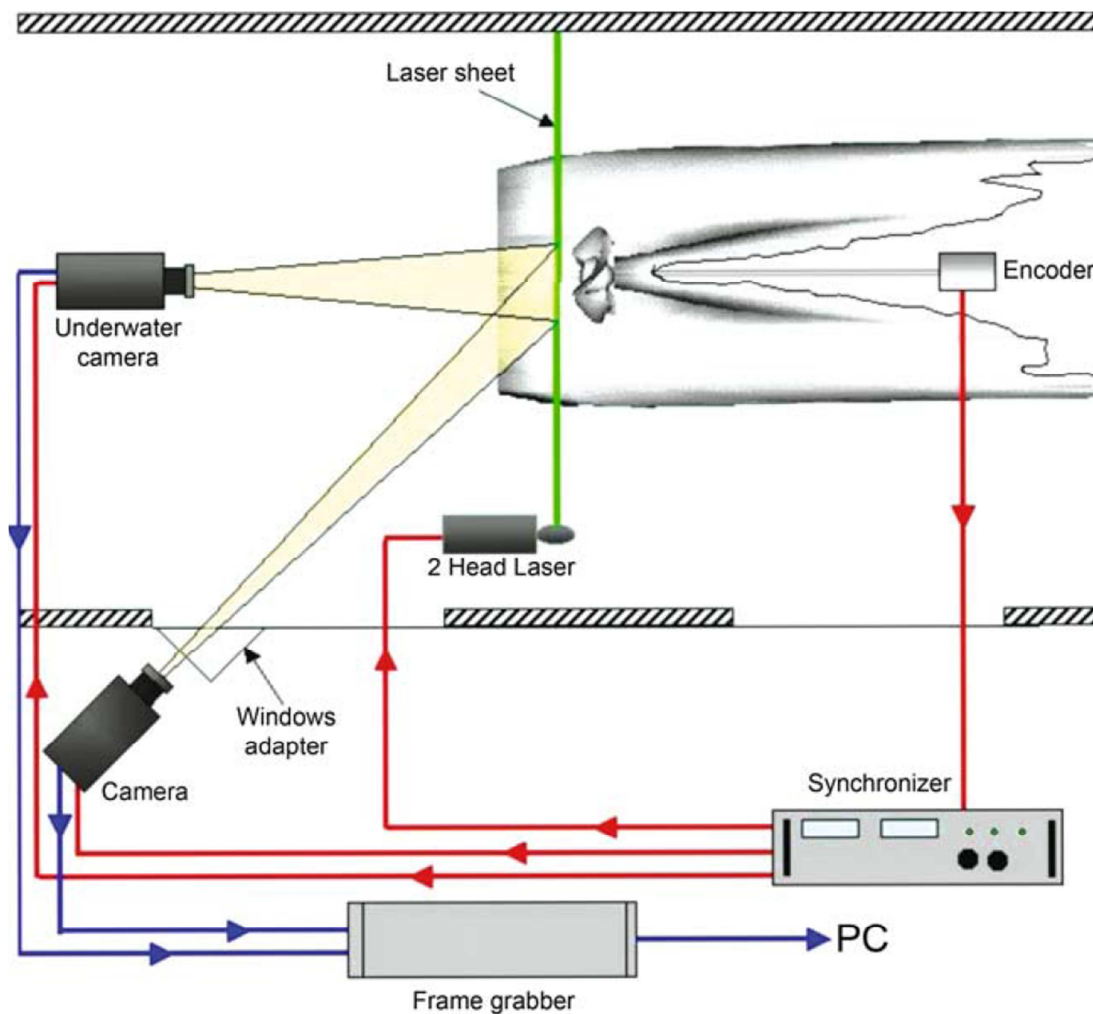


**Figure 3** Sketch of a wet-dry SPIV set-up, [19].

Apart from the mechanical details of the probe, which will be discussed in the next paragraph, this solution is undoubtedly the most effective but is also demanding in either operative and technical terms; in this view, SPIV system components are listed and reviewed briefly to meet requirements imposed by operations inside an underwater probe.

### Cameras

Today, many camera models are present on the market differing in sensor technology, bit and spatial resolution, pixel dimension, acquisition frame rate, sensor dimension and so on; in case of a standard set-up, the selection is based on different factors being driven feasibly by getting the best in terms of performance at the cheapest costs, otherwise when this choice is oriented towards a precise application others factor become the driving ones.

Due to the common dimensions of the models, in the order of magnitude of meters, large areas are generally imaged; thus large sensor formats, that is a high number of pixels, are desirable to attain a good dynamic spatial range [18]. On the other hand, in case camera is fixed inside a case placed at distance from the laser light sheet, having such a large format sensor might implies the use of longer focal objectives thus imaging smaller region of interest; as the consequence, larger cases have to be designed to retain the advantage of using a large format sensor and not waste part of it imaging inside walls of the case or some other part of the underwater probe. Differently, smaller sensors can be used reducing the external dimension of the underwater case, resulting in small disturbances to the flow.

Due to the presence of reflections from the free surface/hull model/ air bubbles, blooming and smearing can easily occur, so camera sensors not affected by these problems should be considered; CCD sensors present slightly better performance in comparison to CMOS [21], [22], even if they are affected by these defects. Recently a new sensor appeared, sCMOS (scientific CMOS, [www.scmos.com](http://www.scmos.com)), based on CMOS with low noise, rapid frame rates and high quantum efficiency; based on these features, sCMOS seems to be best suited for better SPIV measurements in flows with free surface and hull reflections. For operations in towing tanks, due to the limited length, to increase the number

of data per carriage run, higher frequency acquisition is desirable; in this view, these new sCMOS sensor cameras are well suited as its frequency acquisition is sensible higher than classical CCD double shutter ones.

### *Laser source*

Q-switched pulsed lasers are the choice for PIV measurements; when working in large facilities, imaging large regions of interest, high energy lasers are clearly required, in particular for measurements in water. PIV applications in water require an energy density estimated in the range from  $5 \cdot 10^{-4}$  to  $1 \cdot 10^{-3}$  mJ/mm<sup>2</sup> [23], suitable for light sheet thickness of about 1mm seeded with 10  $\mu$ m hollow glass particles. The required energy of the laser source depends on the size of the region to be investigated indeed. For instance, in most towing tank and hydrodynamic applications a 200 mJ laser is normally adequate to investigate areas in the range 100x100 mm<sup>2</sup> to 500x500 mm<sup>2</sup>.

### *Stereo-calibration*

Calibration is a key point for SPIV measurements accuracy; in fact, a misalignment between the target and the laser sheet introduces the largest source of error in the reconstructed velocity components [18]. In large hydrodynamic facilities, aligning accurately the light sheet to the target is obviously more complicated, especially when working in a towing tank and performing deep water measurements. Fortunately, procedures to correct such a source of error have been introduced [15], [24], [17], relaxing this stringent constraint.

At INSEAN an innovative calibrating solution has been proposed [25]; the central feature is that the calibration of the stereoscopic system is based upon the measurement of a calibrated flow. This is achieved through an initial two-dimensional calibration of the measurement plane using a single target point, followed by a perspective and laser sheet thickness optimization that makes use of the measurement of a known reference flow, e.g., a uniform flow. This technique results in planar domain, three-component (2D–3C) measurements with a simpler calibration phase, which delivers uncompromised accuracy, compensates for the mechanical misalignment and eliminates the errors deriving from the classical target plate dot identification. By using this technique, savings in time and costs, due to facility occupation, are assured.

### *Seeding Particles*

For PIV measurements in liquids, seeding particles with tens of microns in diameter are well suited [2], [26]; in particular hollow glass spheres with a diameter of 10-20 micron provide an excellent capability to follow the fluid acceleration and a good light scattering. A critical issue is when large areas have to be seeded; an important amount of tracer and a way to efficiently seed the test section is mandatory; at INSEAN, a devoted tool, a comb-shaped rack, has been developed to add particles over large volumes.

To get better image quality and to eliminate the problem of reflections from hulls, air-water interface and bubbles, fluorescent seeding particles would be the best choice, separating the reflection light, having the same wavelength of the laser source, and the particle scattered light, being fluoresced at a higher wavelength. Unfortunately, this kind of particles presents a serious health threat, being toxic, and are extremely expensive too; in [27], new safe and cheap fluorescent particles are presented, worthy to be considered for large facility applications.

## **A PROBE FOR UNDERWATER MEASUREMENTS**

A highly modular and flexible underwater system for stereoscopic particle image velocimetry measurements has been devised at INSEAN for planar three-dimensional velocity measurements in large-scale facilities such as water tow tanks and tunnels. The underwater SPIV probe is designed in the form of modules that can be assembled into different configurations. Figure 3 shows the probe in its principal configuration, referred to as the design configuration, hosting two cameras. The probe, when fully assembled, forms a streamlined torpedo-like tube with an external diameter of 150 mm. The tube can be rotated about its axis in steps of 15°, and is rigidly linked to a bench through two hydrodynamically optimized struts. The whole system can be attached to the tow-tank carriage or to a traversing system. The components are:

1. two struts; 2. two waterproof-camera sections; 3. two camera mirror sections, opened to water; 4. a waterproof section for the laser light sheet optics; 5. a waterproof section for the light sheet mirror; 6. the nose and tail sections, which have a semi-ellipsoidal shape. The sections are made of stainless steel and are connected together through union couplings and waterproofing is guaranteed by pairs of O-rings on both sides of the couplings.

The stereoscopic system can be assembled in different configurations hosting two or three cameras. The length of the probe in its longest configuration is 2700 mm. The aperture and the focus of the camera lenses are remotely controlled. Each camera head is mounted on a rotation platform that is also remotely controlled for the adjustment of the angle between the axis of the camera optics and the sensor normal axis. This angle, also known as the Scheimpflug angle, allows the camera to focus on a measurement plane that is not perpendicular to the camera optical axis. The

camera housings are ventilated with nitrogen gas to avoid the formation of condensation on the optical parts and on the sensors. Humidity sensors are also fitted in the camera housings, primarily to monitor the presence of water.

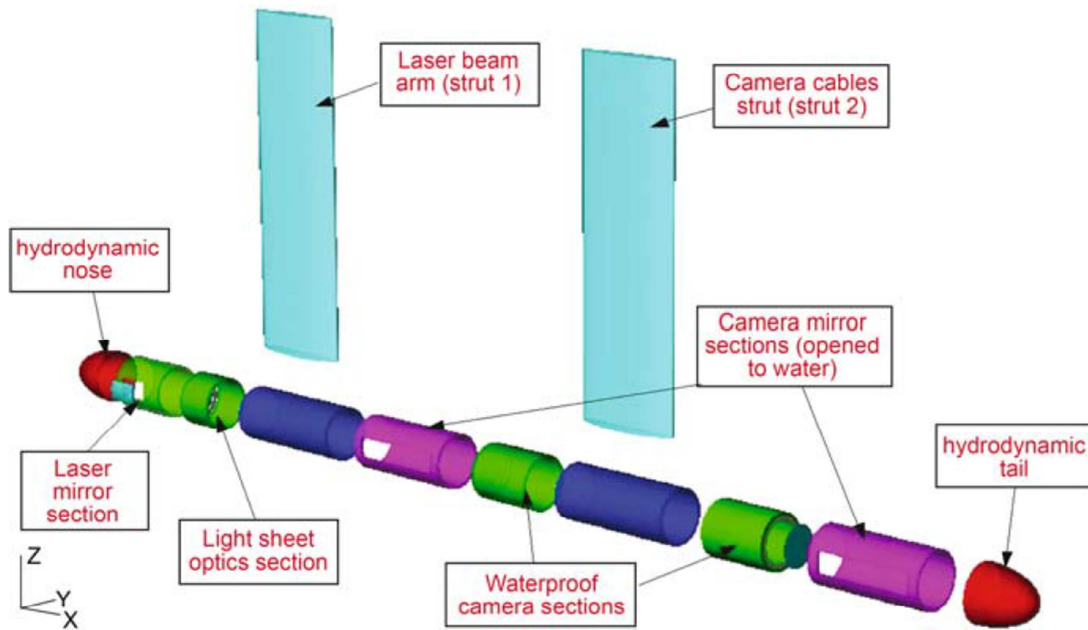


**Figure 4** Sketch of the underwater probe in its two-camera configuration.

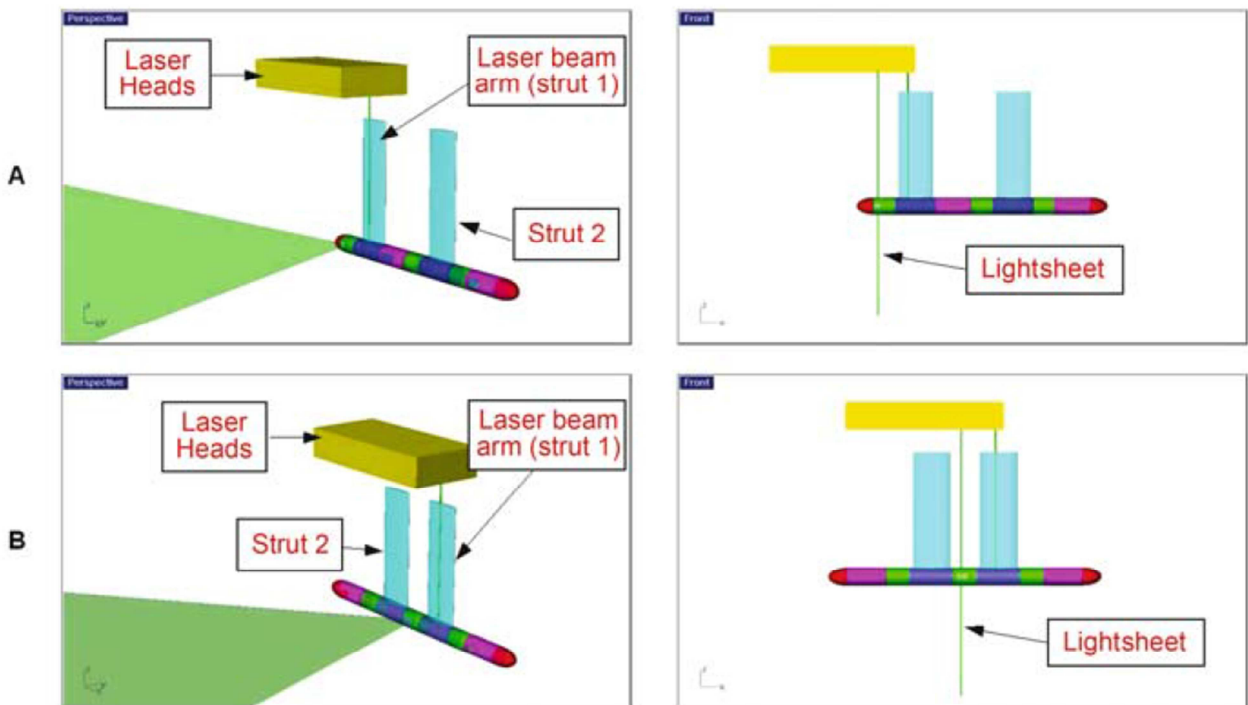


**Figure 5** Underwater probe. A, design configuration. B, symmetric configuration.

The laser light is delivered to the underwater sheet optics through the struts, inside an articulated arm. Mirrors within the arm elbows allow the beam to be correctly driven to the output optics. The laser optics consist of a set of

changeable cylindrical and spherical lenses, which, respectively, expand the beam into a sheet and focus it onto the measurement plane. Each strut also hosts the respective camera cables, as well as those of the corresponding remote control motors and humidity sensor, and the ventilation hose.

The camera mirror sections are opened to water to avoid multimedia refractions, thus minimizing the optical aberrations thanks to the single orthogonal water/air interface. This interface consists of a high optical quality glass window, which also seals the camera section at one end. The mirrors can be manually translated along the probe axis, within their host section, and rotated to adjust the location of the measurement plane and to set the overlap between the two cameras for the stereoscopic configurations. Figure 5 shows four possible configurations of the stereoscopic PIV system. In the main configuration, see Fig. 5A, the cameras are on the same side of the light sheet. This setup is adequate for cross-flow measurements along the hull of a ship model or in the near wake. The arrangement shown in Fig. 5B is suitable for use in the far wake and in the midsections of a ship model. In Figure 6, a picture of the underwater in its three camera configuration is reported.

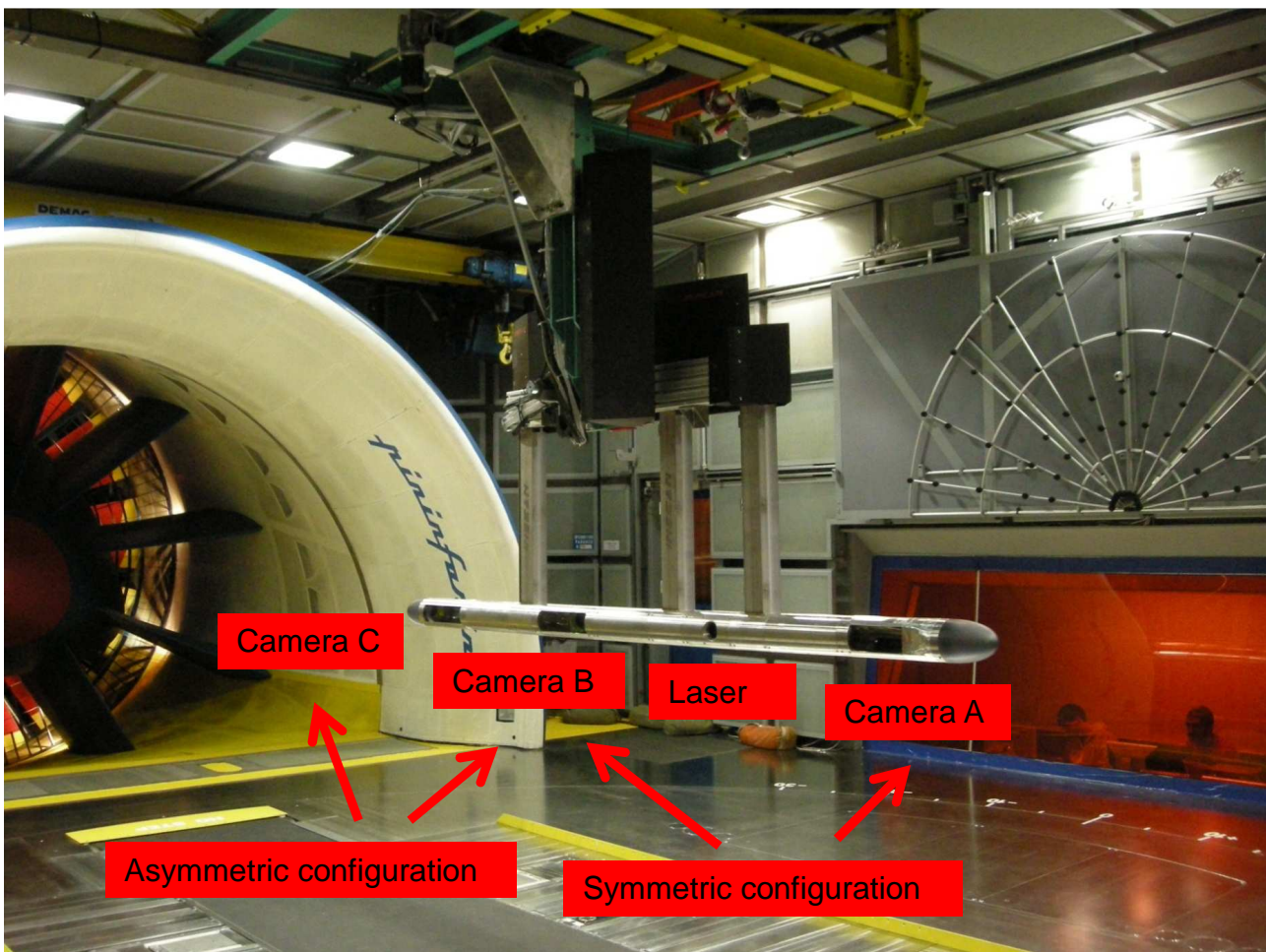


**Figure 6** Underwater probe in its three camera configuration; wind tunnel test set-up.

### TEST CASE: A CATAMARAN IN STEADY DRIFT

In the following, a test case is presented; an overview of the flow around a catamaran model in steady drift has been performed using INSEAN underwater probe. The aim of the work was twofold: the characterization of the strong vortical structures generated along the keel of each demi-hull and to provide a valuable experimental data set for CFD benchmarking in severe off design conditions. Being a two-hull surface ship, measurements were required in the area between the two demi-hulls; problems of reflections, breaking waves, difficult optical access were faced and partially solved. Two speeds, corresponding to  $Fr=0.4$  and  $Fr=0.5$  and to drift angle,  $6^\circ$  and  $9^\circ$ , have been tested. Velocity measurements have been acquired on several cross planes; however, to prevent damages to the PIV system, measurements were taken only on those planes, where ventilation and/or air bubble entrapment did not occur. For the same reason, measurements could not be taken at higher Froude and/or drift angle.

### Catamaran model

As a benchmark case for the work, the Delft372 catamaran form developed by TU Delft [28], [29] was selected as reference geometry and the CNR-INSEAN 2554 model has been built in fiberglass with a scale factor of 1:1. The main particulars of the model and the geometry is shown in Figure 7. In order to stimulate turbulence, the model is equipped with a row of cylindrical studs of 4mm height and 3mm diameter, 30mm spaced, fitted on the model 70mm behind the bow profile.

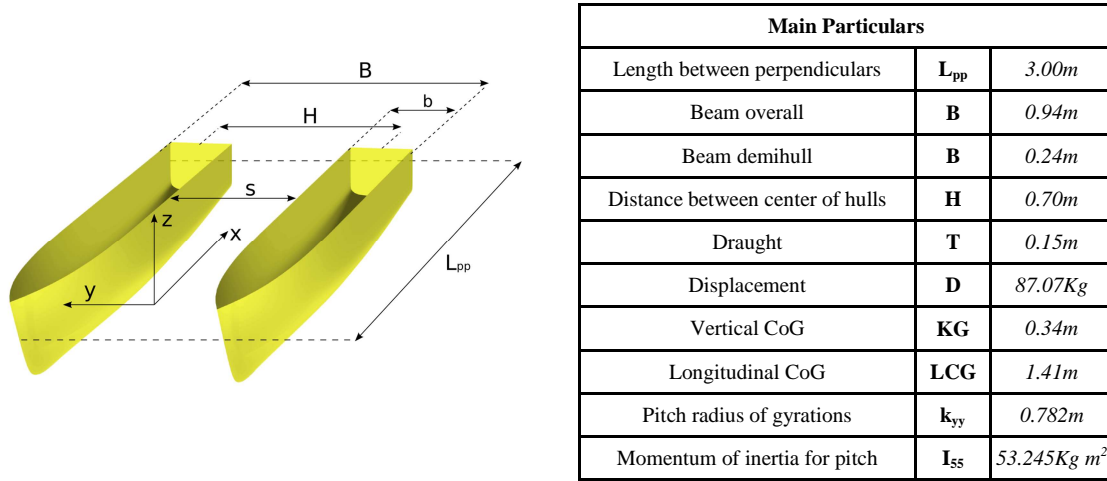


**Figure 7** Catamaran INSEAN-2554: model geometry.

### SPIV hardware

The stereoscopic system consisted of two 11MP CCD sensor cameras, from Illunis LLC, with a pixel resolution of 4000x2672 and 12-bit depth. For this campaign, two Nikon objectives, a Nikkor AF 105mm f/2 D DC and a Nikkor AF 135mm f/2 D DC, were used with an actual f number equal to 16.

The adopted laser supply was the CFR 220 TWINS PIV system by Quantel. This laser system features two small CFR 220 lasers firing side by side at synchronized pulse rate up to 15Hz. The 1064nm energy from each laser head is frequency-doubled and combined into one single beam at the output. The resulting wavelengths are highly pure (>97%) with a 532nm wavelength and a 220mJ energy per pulse.

Hollow glass spheres, 10-20 $\mu$ m in diameter and 1.1 $\pm$ 0.05g/cc in density, have been used as tracer; to uniformly seed the region of interest a system, composed of a stirring tank and a comb-shaped rack, was used.

### Set-up and test matrix

The carriage of towing tank n° 1 is equipped with two couples of rails perfectly aligned to the tank itself; the main couple of rails is fixed permanently and placed on the centerline of the carriage, the secondary couple of rails, which is dismountable, is placed on the left-hand side of the carriage, close to the first one.

The catamaran model was attached to the main rails of the carriage by means of a vertical bar and an angular graduated table; this table assured the geometric alignment to the test section and the correct positioning of the model at the selected drift angle; simultaneously, this system imposed the right sinkage and trim values. Such values were previously evaluated performing PMM (Planar Motion Mechanism) driven tests; this mounting allowed an accurate alignment and fast configuration changes in the x- and y-directions, see Reference system in the following. To minimize the laser beam reflections and improve the signal-to-noise ratio of the PIV images, the model was black painted. To position accurately the laser light sheet at the desired x-coordinate, 4 metallic pins were placed on the hull at known position; the used pins were L-shaped iron pieces inserted directly into the hull.

The underwater probe was mounted on the secondary rails using a 3-axis translation stage; this translation system is a remote controlled 3-axis motion stage with displacement accuracy higher than 0.01mm. The fine alignment and positioning of the probe relative to the model was then ensured by translation stage of the probe itself.

The S-PIV measurements have been performed at planes, Froude numbers and drift angle reported in Table 1. To increase the spatial resolution of the measurement, without reducing the total region of interest, each plane was covered by overlapping a numbers of smaller regions imaged separately.

$\beta$ [deg]	$Fr$	Sinkage ( $z_G/L_{pp}$ )	Trim [deg]
6°	0.40	-5.213E-03	-0.35°
	0.50	-6.86E-03	-1.71°
	0.50	0	0°
9°	0.40	-6.091E-03	-0.19°
	0.50	-8.653E-03	-1.51°

**Table 1** SPIV measurements: test matrix.

$\beta$ [deg]	$Fr$	Plane ( $x/L_{pp}$ )
6°	0.40	0.30, 0.75, 0.95, 1.15, 1.30
	0.50	0.30, 0.75, 0.95
	0.50 (EK)	0.30
9°	0.40	0.30
	0.50	0.30

**Table 2** SPIV measurements: cross planes.

With the used objectives, each patch covered an area, after the stereoscopic reconstruction, equal to 700x300mm<sup>2</sup>. The patches had an overlap ranging between 10% and 65%. For each plane, the translation system was reset to a known reference point on the ship model, given by a calibrated pin. This allowed to reference the model and the translation system to a known relative position and, hence, guaranteed the set-up repeatability of each configuration change. In addition, random checks were made for each plane to insure that the traversing system was working correctly.

Using the mounting flexibility of the probe, the asymmetric configuration was used to perform the whole campaign; to ensure the measurement of the flow near the free surface the probe laser and camera modules have been mounted pointing 15° upward above the horizontal line. The probe was assembled in its two-struts, two camera configuration. The position of the plane where velocity measurements have been taken is reported in Table 2; the distance is taken from the forward perpendicular. Based on the  $L_{pp}$ , the tested velocities are  $V_1=2.170\text{m/s}$  ( $Fr=0.4$ ),  $V_2=2.712\text{m/s}$  ( $Fr=0.5$ ).

#### *Stereoscopic calibration*

A 500x450mm<sup>2</sup> calibration target, consisting of a grid of 23x21 round dots spaced 20mm, was used for the SPIV calibration. The target center was placed at the distance of 1300mm from the probe axis and was mounted on a precision translation stage. The target was used first to calibrate the system in terms of perspective correction for the stereoscopic reconstruction and then to determine the displacement uncertainties along the horizontal in-plane axis and along the normal out-of-plane axis of the target.

The Soloff method based calibration [16] has been used, applying displacement of the calibration target ranging from -5 to +5mm, in steps of 1mm, considering a total of 11 planes z- planes. The stereo-PIV system was calibrated before the measurement campaign and checked at the end by running at constant speed without the model. The difference between the actual and the measured free stream axial velocities was mostly within 3%, with a maximum of 5% in the border regions where the optical aberrations were naturally more important.

#### *Vector field evaluation*

To calculate the instantaneous vector fields, image elaboration has been performed to extract the statistical quantities to be compared with numerical simulations. The whole elaboration has been composed of the following steps:

- image pre-processing operations
- instantaneous velocity fields evaluation on modified images
- validation of velocity fields

- statistical quantities calculation

Due to the presence of hull body and reflections in the acquired images, these have been pre-processed by subtracting the minimum image of each set both on the left and on the right images. This procedure permitted the removal of background and reflections in the images; this operation has been preferred to the mean subtraction because a higher efficiency in the velocity estimation has been obtained due to a better signal to noise ratio. In addition to that with the mean image subtraction, part of the information would have been removed.

After that, the pre-processed images have been analyzed using a standard algorithm, Insight 3G by TSI Inc., based on the cross-correlation operator. This algorithm implements an iterative multi-pass, multigrid, window deformation procedure, with offset and a predictor-corrector strategy. In particular the window offset permits to analyze images with seeding particle displacement larger than the window size so an increase of the spatial resolution is achievable, see [30], [9].

In the iteration steps, a gaussian window is applied to the interrogation window [10]; this procedure is necessary to assure the convergence of the window deformation algorithm and to increase the total frequency response of the operator. In addition to that, generally a bilinear interpolation on the intermediate steps is applied to get a one pixel resolution which is necessary to perform the window deformation and to increase the statistical basis for the cross-correlation evaluation, as in [31].

Overlapping of the interrogation window is also used to obtain a final vector grid as fine as possible; using this feature, a higher spatial resolution is achieved in the stereo reconstruction and flows with strong velocity gradients can be studied.

For the actual study, the final interrogation window was set to 32x32 pixels, with 50% of overlapping. With the used optics, the obtained vector separation is 2.9mm.

To eliminate spurious vectors, i.e. non-physical vectors due to a low signal-to-noise ratio (caused by a low number of particles, borders, reflections and so on), a validation procedure is applied to each instantaneous field; this procedure finds, eliminates and replaces spurious vectors with vectors evaluated on a bilinear interpolation based on the adjacent ones.

In particular, the used procedures are:

- a median filter, to identify displacement vectors exceeding a length or an angle threshold based on the adjacent vectors [32];
- a displacement range based criterion which eliminates and replaces vectors out of the selected interval;
- a topological validation which eliminates and replaces vectors placed in selected regions of the images.

Once the instantaneous left and right vector fields have been evaluated, using a polynomial function based approach for the calibration [16], the 3D-2C instantaneous vector field were reconstructed. On the 3C-2D validated fields, a statistical analysis has been performed to obtain the mean velocity fields, the mean vorticity and other statistical quantities.

## *Results*

Experimental measurements will be presented in the following sections; for a description of the vortical structures generated from the hulls, vorticity fields will be used. Vortex dynamics, with the possibility of instability and/or breakdown will be investigated by the analysis of turbulent quantities, such as vorticity fluctuations and Reynolds stresses.

### *Vorticity fields*

An overview of the vortical structures developing around the hulls is given from Figure 8 to Figure 11, where axial vorticity field is depicted on the cross planes orthogonal to the direction of advancement as reported in Table 2.

Due to the cross flow, two main vortices develop from the keels of both the windward and the leeward hulls; the intensities of these two vortices are similar and they rise up around close to the forward perpendicular. Both vortices are convected toward port side, i.e. they are forced to be aligned with the main flow.

The one from the windward side, is convected in the region between the hulls, therefore strong interaction with the wave system in the inner region is expected. Indeed, as it has been shown in [33], [34] for the catamaran in straight ahead motion, and in [35] in the case of static drift, at this speed a deep wave trough is present in the inner region close to the transom. As a result, in the stern region, the windward vortex is squeezed and pushed down, as it can be seen in Figure 8 and Figure 10 (at section  $x/L_{pp}=0.95$ ). A different dynamics is observed for the leeward vortex; although it remains closer to the free surface it exhibits a lower interaction with the free surface itself.

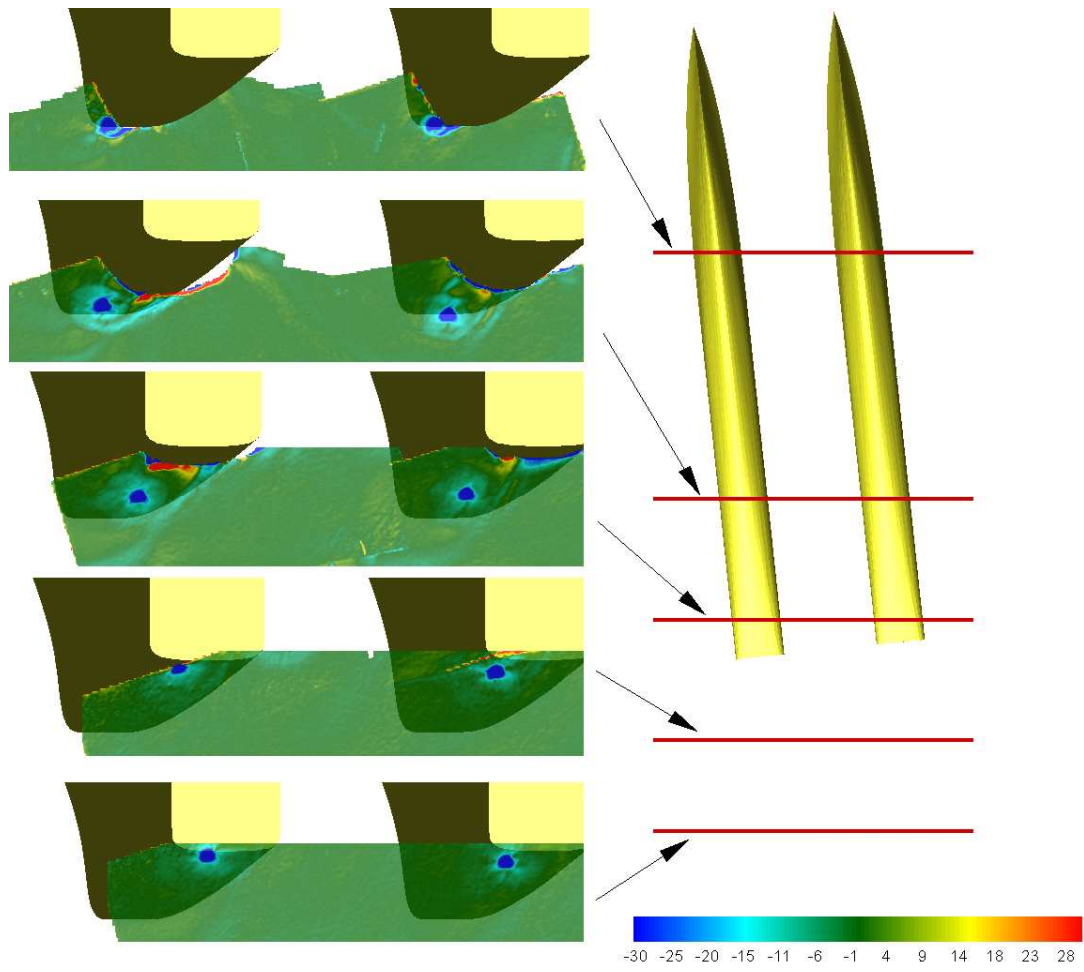


**Figure 8** Vorticity field  $Fr = 0.4$ , drift  $6^\circ$ .

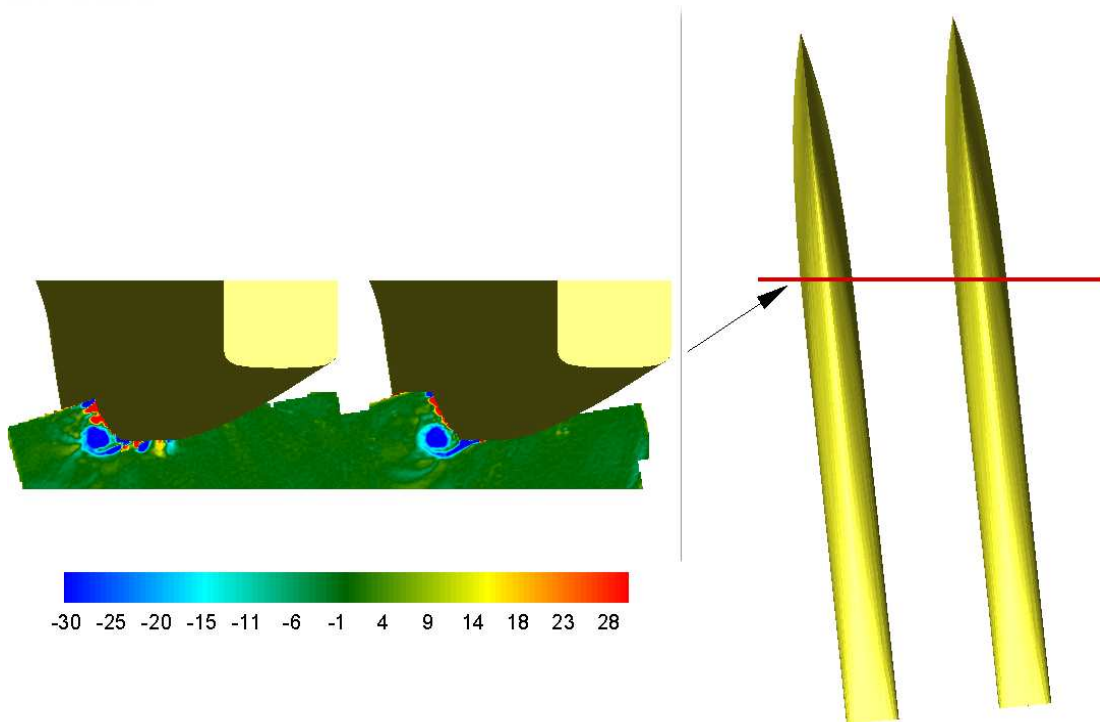


**Figure 9** Vorticity field  $Fr = 0.4$ , drift  $9^\circ$ .

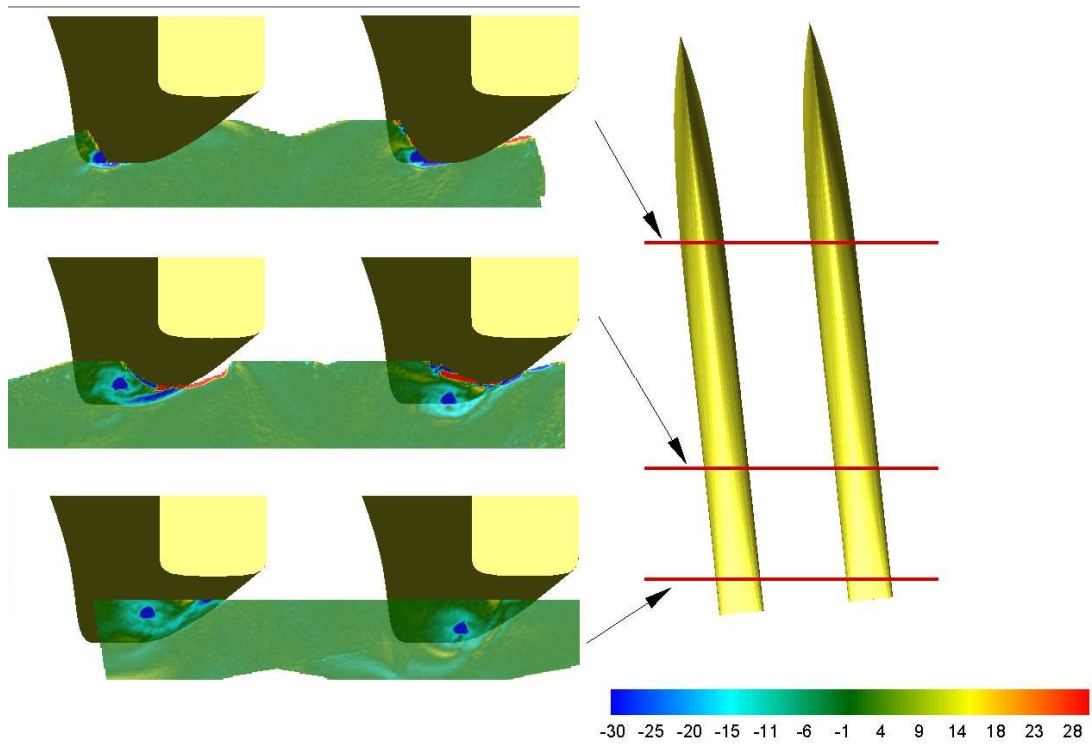


**Figure 10** Vorticity field  $Fr = 0.5$ , drift  $6^\circ$ .

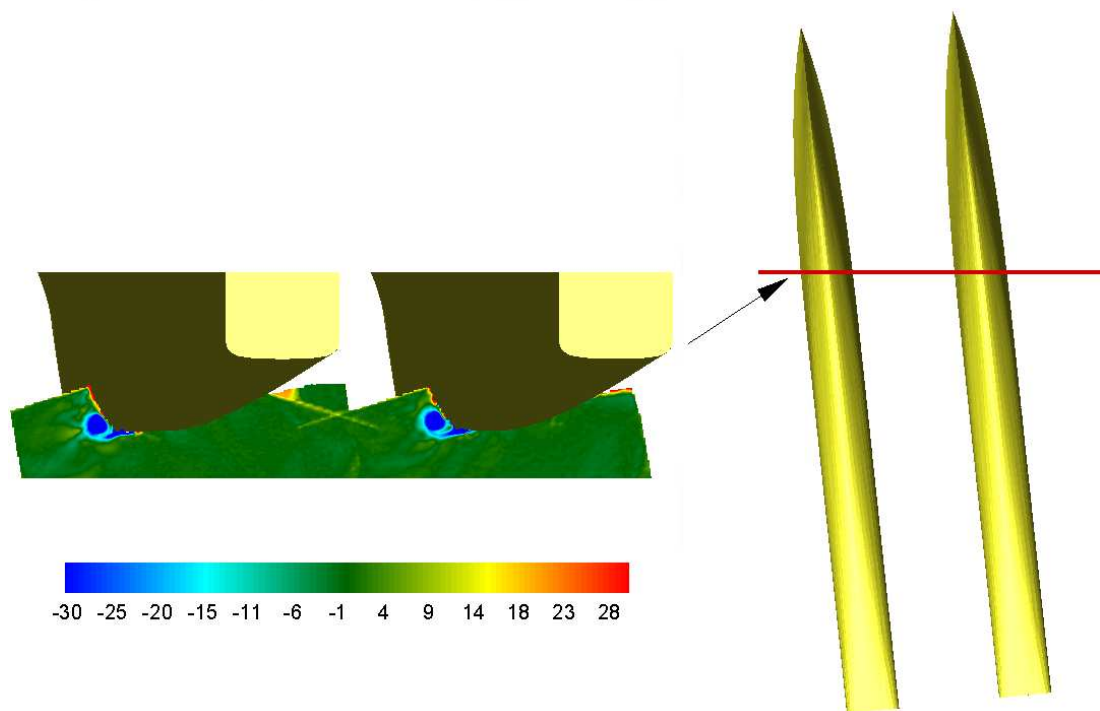


**Figure 11** Vorticity field  $Fr = 0.5$ , drift  $9^\circ$ .

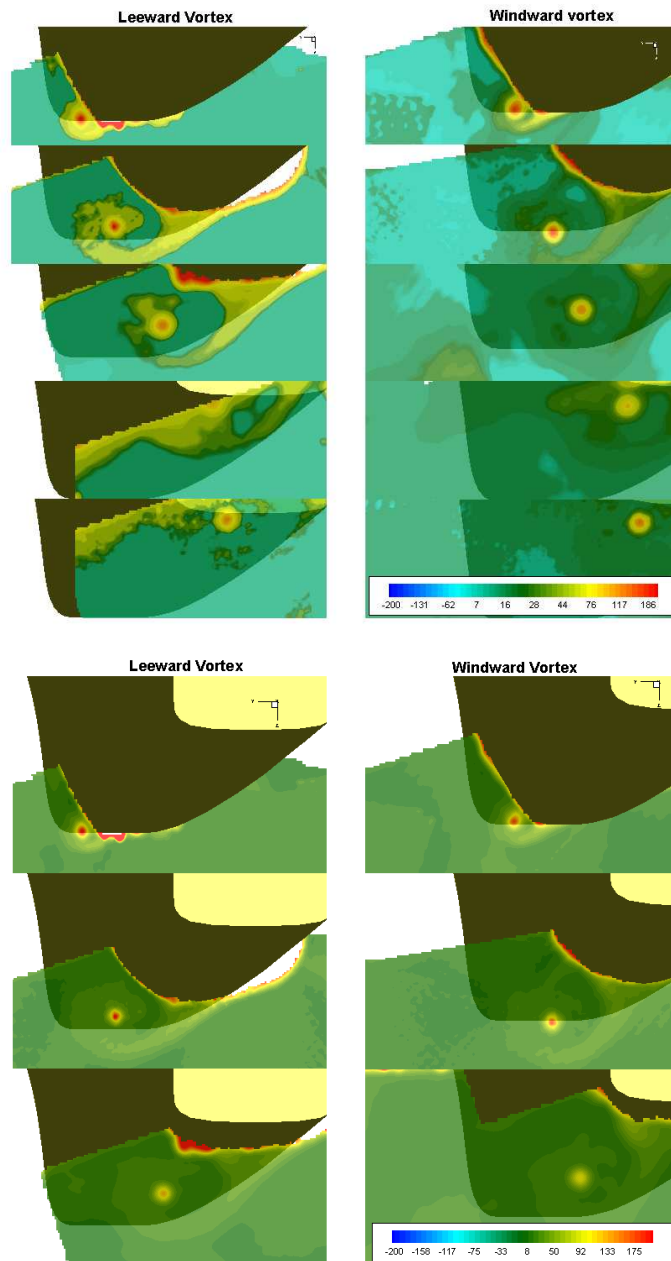


**Figure 12** Standard deviation of the vorticity field for  $Fr = 0.4$  (top) and  $Fr = 0.5$  (bottom). Model at  $\delta = 6^\circ$ .

### *Vorticity fields fluctuations and Reynolds stresses*

The distribution of the vorticity fluctuations is reported in Figure 12 for the cases at  $Fr=0.4$  and  $0.5$  and  $\delta=6^\circ$ . The traces of the standard deviation of the vorticity field in the leeward and windward vortices exhibit nearly the same extent and intensity, with the local maximum at the core region and a quite rapid decay outwards, along the radial direction. This feature highlights the stable nature of the bilge vortices whose positions keep within a very short oscillation amplitude in all the investigated transversal planes. This behavior recurs independently of either the Froude number and the drift angle, at least in the range of conditions considered in the present study.

The analysis of the locus described by the instantaneous traces of the windward vortex centroid in Figure 13 confirms this statement. Indeed, the positions of the vortex centroid keep bounded within the average trace of vortex core and, thus, are far to be considered as indicative of an on-going destabilization process.

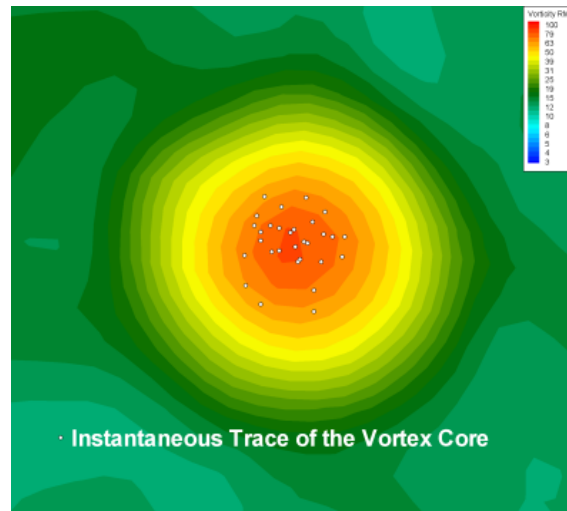


**Figure 13** Locus of the instantaneous traces of the windward vortex centroid. For a better readability just few points are represented.

Figure 14 documents the streamwise evolution of the vorticity fluctuation peak in the bilge vortex core of the windward and leeward demi-hulls. With regard to the bilge vortex behavior, all the curves in Figure 14 do not have a monotone slope and show a different trend with three main regions:

- down to about 70% of the model length, vorticity fluctuations keep about constant.
- from  $0.7L_{pp}$  to about  $1.15L_{pp}$ , vorticity fluctuations exhibit a dramatic reduction to about 40% of the original values. This streamwise reduction is coupled with the more and more larger extent of the vortex trace and, thus, it is to be ascribed to the effect of the turbulent diffusion.
- from  $1.15L_{pp}$  to about  $1.3L_{pp}$ , the increase in the vorticity fluctuations of the bilge vortex core is likely to be the consequence of the wave breaking downstream of the demi-hull and a possible destabilization mechanism of the vortex itself. It is worth noting that this trend was observed only for  $Fr=0.4$ , no experimental data being available downstream of  $x=0.95L_{pp}$  for  $Fr=0.5$ . On the other hand, the very good overlapping between the curves at Froude 0.4 and 0.5 in the range from  $0.3L_{pp}$  to  $0.95L_{pp}$ , makes reasonable the conjecture of a similar behavior also downstream of the model.

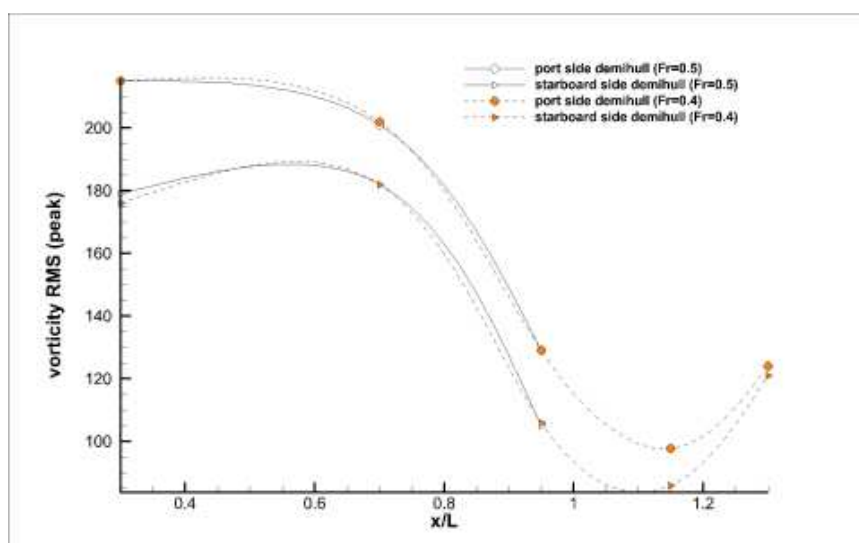


**Figure 14** Streamwise evolution of the vorticity fluctuation peak in the bilge vortex core.

In Figure 15, the same analysis is documented with regard to the vorticity sheet connecting each bilge vortex to the corresponding demi-hull.

In this case, the intensity of the fluctuations in the vorticity sheet reduces monotonically streamwise and tends to approach asymptotically the background level (i.e.  $\omega_{L_{pp}}/U_{\infty}=12-15$ ). The effect of diffusion spreads out the vorticity sheet quite rapidly and fades his trace away downstream of the plane at  $x=0.95L_{pp}$ .

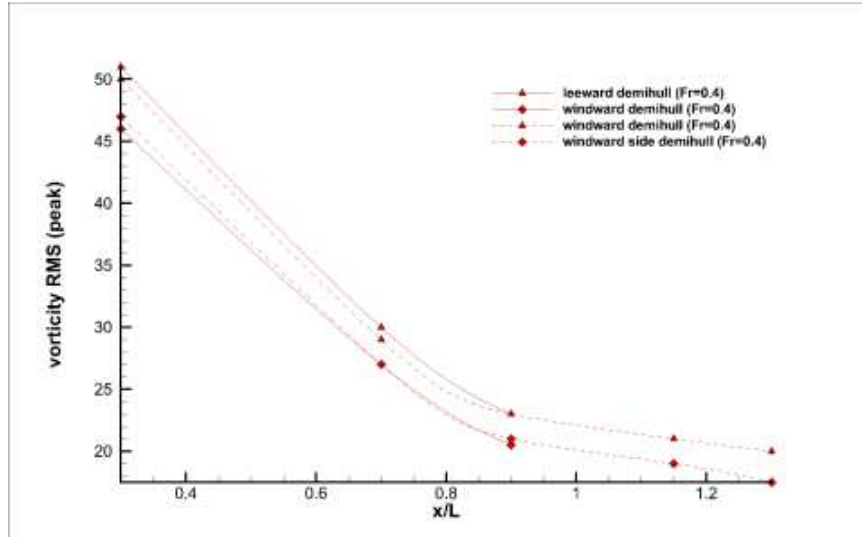


**Figure 15** Streamwise evolution of the vorticity fluctuation peak in the vorticity sheet connecting the bilge vortex to the demi-hull.

This result suggests that the characteristic scales of the eddies forming the vorticity sheet are actually as small as those of the background turbulence.

Figure 16 shows the distribution of the out-of-diagonal terms of the Reynolds Stresses for  $Fr=0.4$  and  $Fr=0.5$  and  $\delta=6^\circ$ .

The largest peaks of the Reynolds stresses correspond to the traces of the bilge vortices, as expected considering that the shear stresses are maximum locally. The diffusive action of the turbulence smooths the velocity gradients quite rapidly streamwise and consequently results in a rapid decay of the Reynolds stresses. More specifically, stresses in the bilge vortex region undergo an abrupt decay downstream of plane P2 (i.e.  $x=0.7L_{pp}$ ) and are almost faded away at plane P4.

Similarly to what observed in Figure 12 for the vorticity fluctuations, the intensity of the Reynolds stresses appears increased at  $x=1.3L_{pp}$ . This result is a further evidence of the possible destabilization mechanism of the bilge vortex downstream of the model, as might be considering that the local increase of the Reynolds stresses identifies regions in which turbulence and instabilities are typically generated [36].

## CONCLUSIONS

Critical issues of the application of SPIV in large hydrodynamic facilities have been discussed and an underwater probe suitable to investigate flows of naval interest is presented. As a test case, this SPIV system has been used for the measurements of the velocity field around a catamaran, namely the Delft 372 model, for which a large database is in construction through other projects. Velocity measurements have been taken for two speeds (corresponding to  $Fr=0.4$  and  $0.5$ ) and two drift angles (6 and 9 degrees) on several planes in the region between the hulls and the outer region of the leeward hull have. A description of the vortical structures generated from the hulls has been done using vorticity fields. Vortex dynamics has been successfully investigated by the analysis of turbulent quantities, such as vorticity fluctuations and Reynolds stresses.

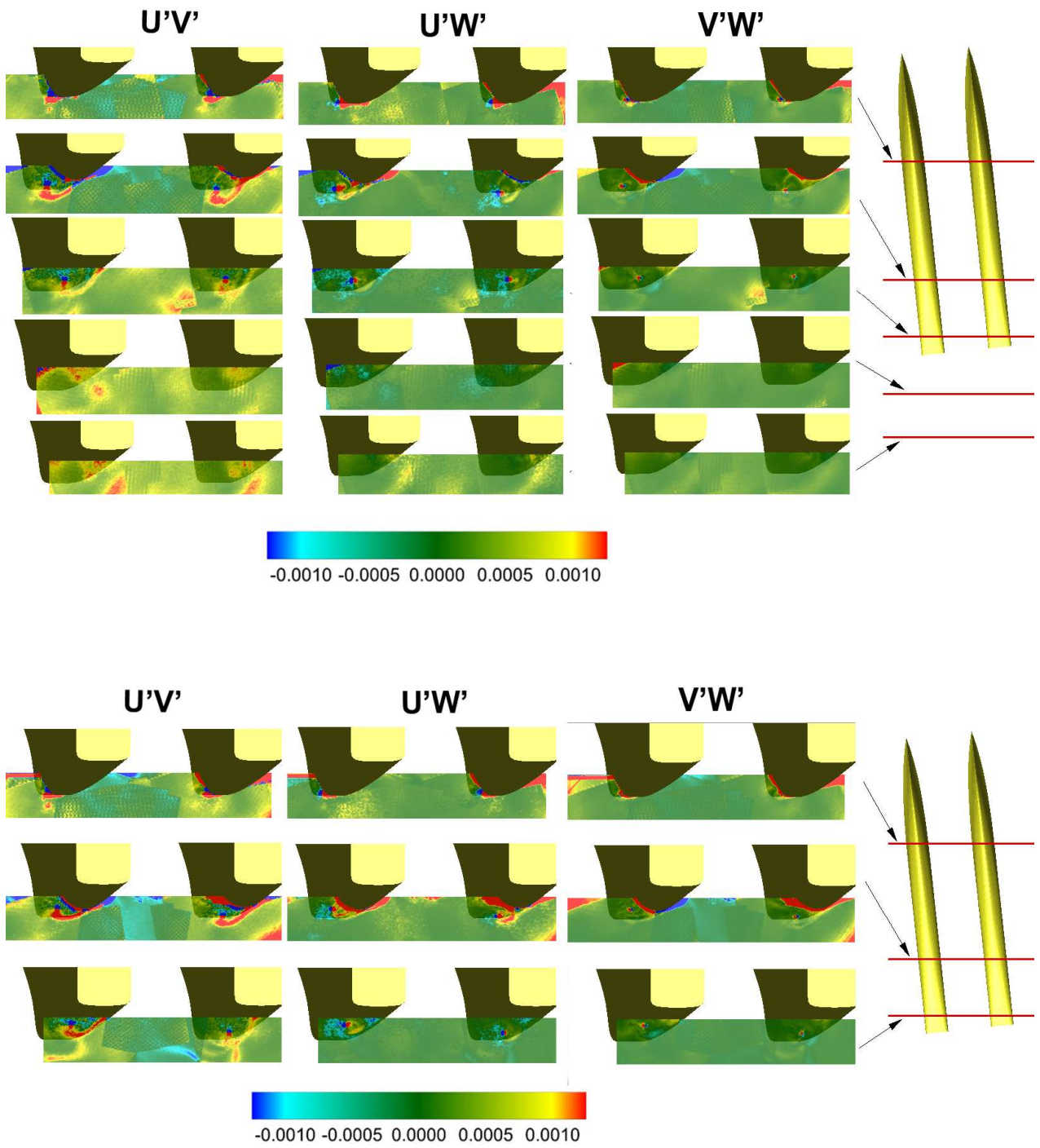


**Figure 16** Distribution of the out-of-diagonal terms of the Reynolds stresses for  $Fr = 0.4$  (top) and  $Fr = 0.5$  (bottom). Model at  $\delta = 6^\circ$ .

## ACKNOWLEDGMENTS

The activities reported here have been partially funded by the U.S. Office of Naval research, through Dr. L. Patrick Purtell in the framework of the NICOP project "*Complementary EFD and CFD Analysis of Calm Water Hydrodynamics and Large Amplitude Motion for High-Speed Catamarans*".

## REFERENCES

- [1] Tupper EC "Introduction to Naval Architecture" Elsevier (2004).
- [2] Adrian RJ "Scattering particle characteristics and their effect on pulsed laser measurements of fluid flow: speckle velocimetry vs. particle image velocimetry" *Applied Optics* (1984), Vol.23, pp. 1690-1691.
- [3] Adrian RJ "Multi-point optical measurements of simultaneous vectors in unsteady flow – a review" *International Journal of Heat and Fluid Flow* (1986), Vol. 5, pp. 127-146.
- [4] Lourenco LM, Goginemi SP, Lasalle RT "On-line particle image velocimeter: an integrated approach" *Applied Optics* (1994), Vol. 33, pp. 2465-2470.
- [5] Keane RD, Adrian RJ "Theory of cross-correlation analysis of PIV images" *Applied Scientific Research* (1992), Vol. 49, pp. 191-215.
- [6] Keane RD, Adrian RJ, Zhong Y "Super-resolution particle-imaging velocimetry" *Measurement Science and Technology* (1995), Vol. 6, pp. 754-768.
- [7] Takehara K, Adrian RJ, Etoh GT, Christensen KT "A Kalman tracker for super-resolution PIV" *Experiments in Fluids* (2001), S34-S41.
- [8] Hart DP "PIV error correction" *Experiments in Fluids* (2000), Vol. 29, pp. 13-22.
- [9] Scarano F "Iterative image deformation methods in PIV" *Measurement Science and Technology* (2002), Vol. 13, R1-R19.
- [10] Di Florio D, Di Felice F, Romano GP "Windowing, re-shaping and re-orientation interrogation windows in PIV for the investigation of shear flows" *Measurement Science and Technology* (2002), Vol.13, pp. 953-962.
- [11] Astarita T "Analysis of weighting windows for image deformation methods in PIV" *Experiments in Fluids* (2007), Vol. 43, pp. 859-872.
- [12] Prasad AK, Adrian RJ "Stereoscopic particle image velocimetry applied to liquid flows" *Experiments in Fluids* (1993), Vol. 15, pp. 49-60.
- [13] Zhang W, Prasad AK "Performance evaluation of a Scheimpflug stereocamera for particle image velocimetry" *Applied Optics* (1997), Vol. 36, pp. 8738-8744.
- [14] Tsai RY "An efficient and accurate camera calibration technique for 3D machine vision" *Proceedings of the IEEE conference on computer vision and pattern recognition (CVPR'86)*, Miami, Florida, pp. 364-374.
- [15] Willert CE "Stereoscopic digital particle image velocimetry for application in wind tunnel flows" *Measurement Science and Technology* (1997), Vol. 8, pp. 1465-1479.
- [16] Soloff SM, Adrian RJ, Liu ZC "Distorsion compensation for generalized stereoscopic particle image velocimetry" *Measurement Science and Technology* (1997), Vol. 8, pp. 1441-1454.
- [17] Wieneke B "Stereo-PIV using self-calibration on particle images" *Experiments in Fluids* (2005), Vol. 39, pp. 267-280.
- [18] van Doorne CWH, Westerweel J "Measurement of laminar, transitional and turbulent pipe flow" *Experiments in Fluids* (2007), Vol. 42, pp. 259-279.
- [19] Schroder A, Willert CE "Particle Image Velocimetry – New Developments and Recent Applications" Springer (2007).
- [20] Raffel M, Willert CE, Werely S, Kompenhans J "Particle Image Velocimetry – A Practical Guide" Springer (2007).
- [21] Hain R, Kahler CJ, Tropea C "Comparison of CCD, CMOS and intensified cameras" *Experiments in Fluids* (2007), Vol. 42, pp. 403-411.
- [22] Falchi M, Romano GP "Evaluation of performance of high speed PIV compared to standard PIV in a turbulent jet" *Experiments in Fluids* (2009), Vol. 47, pp. 509-526 .
- [23] *Proceedings of the 26<sup>th</sup> International Towing Tank Conference – Detailed Flow Measurements Committee*, Rio de Janeiro, Brazil, 28<sup>th</sup> August – 3<sup>rd</sup> September, 2011
- [24] Coudert SJM, Schon JP "Back-projection algorithm with misalignment corrections for 2D3C stereoscopic PIV" *Measurement Science and Technology* (2001), Vol. 12, pp. 1371-1381.
- [25] Grizzi S, Pereira AFJ, Di Felice F "A simplified, flow-based calibration method for stereoscopic PIV" *Experiments in Fluids* (2010), Vol. 48, pp. 473-486.
- [26] Westerweel J, Elsinga GE, Adrian RJ "Particle Image Velocimetry for Complex and Turbulent Flows" *Annual Review of Fluid Mechanics* (2013), Vol. 45, pp. 409-436.
- [27] Pedocchi F, Martin JE, Garcia MH "Inexpensive fluorescent particles for large-scale experiments using particle image velocimetry" *Experiments in Fluids* (2008), Vol. 45, pp. 183-186.
- [28] van't Veer, R. "Experimental results of motions and structural loads on the 372 catamaran model in head and oblique waves" *Technical Report* (1998). TU Delft, Report N.1130.
- [29] van't Veer, R. "Experimental results of motions, hydrodynamic coefficients and wave loads on the 372 Catamaran model" *Technical Report* (1998). TU Delft, Report N.1129.
- [30] Westerweel J. "Fundamentals of Digital Particle Image Velocimetry", *Measurement Science and Technology* (1997), Vol.8, pp.1379-1392.
- [31] Astarita T. "Analysis of weighting windows for image deformation methods in PIV", *Experiments in Fluids* (2007), Vol. 43, pp. 859 - 872.
- [32] Westerweel J. "Efficient detection of spurious vectors in particle image velocimetry data", *Experiments in Fluids* (1994), Vol.16, pp. 236 -247.
- [33] Stern F, Carrica P, Kandasamy M, Gorski J, ODea J, Hughes M, Mille, R, Hendrix D, Kring D, Milewski W, Hoffman R, Cary C, "Computational hydrodynamic tools for high-speed sealift". *SNAME* (2006), Trans. 114, pp. 55–81.
- [34] Broglia R, Bouscasse B, Jacob B, Olivieri A, Zaghi S, Stern F "Calm Water and Sea keeping Investigation for a Fast Catamaran", 11th International Conference on Fast Sea Transportation FAST 2011, Honolulu, Hawaii, USA, September 2011.

- [35] Zlatev ZZ, Milanov E, Chotukova V, Sakamoto N, Stern F. "Combined Model-Scale EFD-CFD Investigation of the Maneuvering Characteristics of a High Speed Catamaran", Proceedings. Of the 10<sup>th</sup> International Conference on Fast Sea Transportation, FAST2009, 5-9 October, 2009, Athens, Greece, Vol. 1, pp. 449-462.
- [36] Tennekes H, Lumley JL, "A First Course in Turbulence" MIT Press, Cambridge (1982).